SHORT-TERM VARIABILITY OF GAMMA RADIATION AT THE ARM EASTERN NORTH ATLANTIC FACILITY (AZORES)

S. M. Barbosa[a], P. Miranda[b], E. B. Azevedo[c]

[a] INESC TEC - INESC Technology and Science, Porto, Portugal

[b] University of Lisbon, Instituto Dom Luiz, Lisboa, Portugal

[c] Center of Climate Meteorology and Global Change, University of the Azores

Corresponding author:

Susana M. Barbosa

susana.a.barbosa@inesctec.pt

INESC TEC, Campus da FEUP,

R Dr Roberto Frias, 4200-465 Porto

Tel: +351 22 209 4129

Fax: +351 22 209 4050

ABSTRACT

This work addresses the short-term variability of gamma radiation measured continuously at the Eastern North Atlantic (ENA) facility located in the Graciosa island (Azores, 39N; 28W), a fixed site of the Atmospheric Radiation Measurement programme (ARM). The temporal variability of gamma radiation is characterized by occasional anomalies over a slowly-varying signal. Sharp peaks lasting typically 2-4 hours are coincident with heavy precipitation and result from the scavenging effect of precipitation bringing radon progeny from the upper levels to the ground surface. However the connection between gamma variability and precipitation is not straightforward as a result of the complex interplay of factors such as the precipitation intensity, the PBL height, the cloud's base height and thickness, or the air mass origin and atmospheric concentration of sub-micron aerosols, which influence the scavenging processes and therefore the concentration of radon progeny. Convective precipitation associated with cumuliform clouds forming under conditions of warming of the ground relative to the air does not produce enhancements in gamma radiation, since the drop growing process is dominated by the fast accretion of liquid water, resulting in the reduction of the concentration of radionuclides by dilution. Events of convective precipitation further contribute to a reduction in gamma counts by inhibiting radon release from the soil surface and by attenuating gamma rays from all gamma-emitting elements on the ground. Anomalies occurring in the absence of precipitation are found to be associated with a diurnal cycle of maximum gamma counts before sunrise decreasing to a minimum in the evening, which are observed in conditions of thermal stability and very weak winds enabling the build-up of near surface radon progeny during the night.

Keywords (max 6): gamma radiation; radon; aerosols; precipitation; ARM programme;

1. Introduction

The omnipresence of Radon (Rn-222) in natural environments, its noble gas nature, and its half-life of 3.8 days, make it particularly suitable as a natural environmental tracer in diverse geoscience applications (e.g. Barbosa et al. 2015). Radon has been extensively used as an atmospheric tracer (Wilkening, 1981), including as an indicator of atmospheric turbulence (e.g. Sesana et al. 2006) and as a tool to characterize the nocturnal stable boundary layer (e.g. Williams et al. 2013). Radon measurements over the oceans have been used to identify radon-rich air masses that have originated from continental areas (e.g. Arnold et al. 2009; Chambers et al. 2009), particularly in remote oceanic locations such as the Hawaii (Whittlestone et al. 1992; Chambers et al. 2013).

Continuous radon monitoring, particularly in the case of very low concentrations such as typically found in the atmosphere, is much more challenging than the continuous monitoring of radon progeny, fostering the measurement of the gamma radiation from the radioactive decay of radon progeny as an alternative to the direct measurement of radon. Crystal scintillators for gamma rays have higher relative sensitivity in comparison to solid-state alpha detectors and ionization chambers, allowing for a more detailed characterization of the temporal variability of environmental radioactivity, particularly in the case of fast changes (Zafrir et al. 2011).

In the present study the temporal variability of gamma radiation is examined at a remote oceanic site, on a small island in the middle of the North Atlantic Ocean (Graciosa island, Azores). The specific geographical location of the site is a crucial aspect of the study. Graciosa is sufficiently remote to be clear of direct continental influence (~1500 km from Europe) and typically experiences relatively clean conditions advected from the central North Atlantic, but is also subject to periodic episodes of continentally influenced polluted air masses from Western Europe, North Africa, and North America (Logan et al. 2014; Wood et al. 2015). Continuous monitoring of gamma radiation is carried out at the Eastern North Atlantic (ENA) facility, a fixed site of the Atmospheric Radiation Measurement programme (ARM), established and supported by the Department of Energy (DOE) of the United States of America with the collaboration of the local government and University of the Azores. The collection of data at the ENA facility ensures the existence of detailed knowledge on the atmospheric conditions at the site (Rémillard et al. 2012; Dong et al. 2014; Mann et al. 2014) and the availability of a comprehensive suite of very detailed and high-quality atmospheric measurements that can be used as unique source of ancillary observations for the interpretation of the radiation measurements.

Gamma radiation measured in the air at ~1m above the ground (the standard height for gamma dose rate measurements) comprises gamma rays from both the surface and the atmosphere. The largest surface contribution is from gamma rays originating inside mineral grains in the soil matrix, either from the long-lived gamma-emitting elements (K-40, U-238, Th-232) or from Rn-222 and its progeny, and is therefore stable in time, since the concentration of radionuclides inside the mineral grains is constant in time. The surface contribution also includes radon atoms emanated from the solid grains to the air or water-filled space of the porous medium which varies in time according to the overall up or downward transport of radon inside the porous medium. The atmospheric

contribution includes gamma rays emitted by radon gas progeny in the near-surface atmosphere as well as progeny brought down from the upper atmosphere by below-cloud wash-out and in-cloud scavenging by nucleation or impaction (e.g. Levin and Cotton, 2008). Stratiform and stratocumulus clouds (Wood, 2012) typically at low height and with small thickness, are limited to scavenge radon progeny within the boundary layer, while dynamically active cumuliform clouds with high cloud tops are able to scavenge radon progeny from the troposphere.

This study focus on the short-term variability (daily and sub-daily time scales) of gamma radiation measured continuously at the ARM-ENA facility, and its association with atmospheric conditions. The temporal variability of gamma radiation has been repeatedly addressed (e.g. Minato, 1980; Takeuchi and Katase, 1982; Inomata et al. 2007; Mercier et al. 2009; Yakovleva et al. 2016) as it is a crucial aspect in practical applications such as the routine monitoring of nuclear facilities. In this environmental surveillance context it is fundamental to discriminate between increased levels of gamma radiation associated with artificial radioactivity, and the natural variability in gamma radiation associated with specific atmospheric conditions such as the occurrence of precipitation. Furthermore, the scientific applications relying on radionuclides as atmospheric tracers require a detailed understanding of the different processes influencing their variability. Several studies reported strong short-term variations in environmental gamma radiation associated with precipitation, but its dependence with the rate, duration and amount of precipitation is found to be highly variable (Fujinami, 1996; Inomata et al. 2007; Burnett et al. 2010). Furthermore, strong enhancements in gamma rays have been reported even in the absence of precipitation (Inomata et al. 2007; Yakovleva et al. 2016) as well as cases of precipitation events producing no detectable effects in the gamma radiation, and interpreted as the result of the distance between the precipitation measuring station and the gamma monitoring site (Yakovleva et al. 2016). An obvious hindrance of previous studies is the lack of temporal and/or spatial resolution of gamma and meteorological measurements, for example relying on hourly averaged precipitation (e.g. Inomata et al. 2007) or precipitation data collected only once every 12 h (Yakovleva et al. 2016). Another evident limitation is the noncontiguous location of gamma and precipitation measurements (e.g. Yakovleva et al. 2016).

Here the link between gamma radiation short-term peaks and precipitation is investigated in-depth taking advantage of the extensive meteorological infrastructure available at the ARM-ENA site. The monitoring site is described in section 2.1, the instrumental set-up is depicted in section 2.2., and the data used in the study are presented in section 2.3. The results are shown in section 3 and discussed in section 4, along with concluding remarks.

2. Material and methods

2.1. Geographical setting

The Graciosa Island (39 ºN 28 ºW) is the second smallest island of the Azores Archipelago (Portugal). It is a small (~60 km^2 area) and low lying (~400m) volcanic island dominated by a 1.6 km wide central caldera in the southeast (Fig. 1). As a result of its location between the subtropics

and the mid latitudes, Graciosa experiences a diverse range of air mass histories and is subject to strong synoptic meteorological variability including cyclonic systems, fronts, and periods of extensive low-level cloudiness. The island is small and low enough that clouds above are not strongly influenced by its presence, making it a very suitable site for the study of the Marine Boundary Layer (MBL). While not subject to direct continental influence because of its remote oceanic location, Graciosa experiences in addition to pristine arctic air masses from the north also air masses that have been circulating around the Azores high pressure system over the ocean for several days as well as markedly polluted continental air masses from both North America and Europe, making it a very suitable site for studies on aerosols and microphysical cloud properties (Wood et al. 2009).

Following the deployment of the ARM mobile facility at Graciosa (2009-2010) in the context of the Clouds, Aerosol and Precipitation in the Marine Boundary Layer (CAP-MBL) field campaign (Wood et al. 2015), a new fixed facility became operational at Graciosa Island at the end of 2013 (Nitschke et al. 2014). The gamma radiation monitoring field campaign at the ARM-ENA facility was initiated in May 2015 and is expected to run continuously up to March 2018.

2.2. Instrumental set-up

Continuous monitoring of gamma rays is performed using an NaI(Tl) scintillation sensor of 3” x 3” (Scionix, Holland) equipped with an electronic total count Single Channel Analyzer (SCA) measuring gamma radiation in the range 475 KeV to 3000 KeV. The instrument is placed inside a metal container (6 m length, 2.44m width and 2.55m height) sitting 15 cm above a concrete slab of 25 cm depth. The sensor is placed vertically, looking upwards, at a height of 1.025 m from the container floor. The total count of gamma rays registered by the scintillator is recorded every 15 minutes.

The gamma scintillator measures the gamma radiation from the radioactive decay of the radon progeny, Pb-214 (half-life 26.8 min) and Bi-214 (half-life 19.9 min), as well as the contribution from very long-lived radionuclides U-238, Th-232 and K-40. An additional potential source of gamma rays is the secondary radiation from atmospheric interactions with cosmic rays (Brunetti et al. 2000; Dorman, 2013). However, higher resolution measurements (e.g. 1-minute instead of 15-minutes) would be preferable to detect that contribution.

2.3. Data

Data from the gamma radiation monitoring campaign at the ARM-ENA facility are considered for the period from day 128 (2015-05-08) to day 164 (2015-06-13). The time series of counts per minute (cpm) for every 15-minutes is displayed in Fig. 2. A running median with a window of 3 observations (45 minutes) is applied to the raw measurements for minimal robust smoothing and elimination of eventual isolated outliers (Härdle and Steiger, 1995), such as the ones associated with secondary cosmic rays. Furthermore, the long-term variability signal (represented by the

smooth curve in Fig. 2) is estimated by locally-weighted polynomial regression using the lowess algorithm (Cleveland, 1979). This slowly-varying signal in gamma radiation, with higher counts in the middle (and drier) part of the record, is likely determined by the moisture content of the surface and the resulting attenuation of gamma rays from the terrestrial radionuclides (K, U, Th). Since the focus of the present study is on short-term variability, this long-term signal is subtracted from the time series and the absolute counts are converted to relative counts (%) using a mean value of 7550 cpm. This detrended time series (Fig. 3) is considered hereafter.

Meteorological ancillary data at the monitoring site are obtained from the ARM Data Archive. These include atmospheric pressure, air temperature, relative humidity, visibility, wind speed and wind direction from ARM standard meteorological instrumentation at surface (MET datastream); precipitation and hydrometeor's characteristics from OTT Parsivel2 laser disdrometer (PARS datastream); concentration of aerosol from Humidified Tandem Differential Mobility Analyzer (AOSHTDMA datastream); atmospheric boundary layer height from ceilometer (CEIL datastream); cloud height above ground level from Micropulse Lidar cloud mask (MPLCMASK value added product); and CAPE (convective available potential energy) derived from microwave radiometer profiler measurements (MWRP datastream). Although the sampling rate of the meteorological time series is higher than the 15-minute rate of the gamma radiation series, the original ~10-min rate of the AOSHTDMA data and the 1-min rate of all the other variables is kept unchanged in order to avoid the modification of temporal variability patterns that could result from temporal aggregation of the observations.

All times are UTC (Coordinated Universal Time). All gamma and meteorological data are freely available from the ARM data archive.

3. Results

The time series of variations in gamma radiation counts exhibits changes typically below 5% (Fig. 3). However, the series displays very clear peaks, and despite the low percentage variation (3%-6%) these anomalies are statistically significant and well above the average noise (<< 1%). Two types of anomalies can be distinguished: sharp peaks (e.g. days 128, 129, 133, 161) lasting a few hours, and broader peaks (e.g. days 141, 142, 150,153, 154, 156). Troughs are smaller in magnitude and less common and mostly occur after a sharp peak (e.g. days 128, 162), although there are exceptions (e.g. days 155, 160). Two periods characterized by very low volatility and absence of anomalies can be clearly identified from 14th to 20th May 2015 (days 134 to 140) and from May 23rd to 29th (days 143 to 149).

Atmospheric conditions are expected to strongly influence the concentration of radon progeny in the atmosphere and therefore the variability of gamma radiation counts. The state of the atmosphere during the monitoring period is addressed in section 3.1, and a detailed assessment of its influence on gamma radiation short-term variability is presented in section 3.2.

3.1. Atmospheric conditions

Surface atmospheric conditions for the period under consideration are examined from the time series of basic surface meteorological observations at the ENA facility (Fig. 4). The temporal evolution of atmospheric pressure (Fig. 4 (a)) indicates three distinct periods: a first period of mainly stormy weather, from 8th to 13th May (days 128 to 133), characterized by very low atmospheric pressure; an intermediate period of mainly fair weather, from 14th to 30th May (days 134 to 150), dominated by high atmospheric pressure; and a lower pressure period from 31st May onward. A corresponding distinction is evident in the other meteorological variables: in the 1st period the air temperature is lower and with an irregular diurnal cycle (Fig. 4 (b)) and winds are typically strong (Fig. 4 (c)) and from the S-SW (Fig. 4 (d)); the intermediate period is characterized by consistent diurnal temperature variability and stable easterly winds; the final period is associated with warmer weather and mainly westerly winds. The properties of clouds are also markedly different for the three periods, particularly in terms of cloud base height (Fig. 5 (a)), the middle part of the record being characterized by low as well as thinner (Fig. 5 (b)) clouds. The height of the Planetary Boundary Layer (PBL) separating the free atmosphere from the atmosphere responding to surface forcings also tends to be lower in the intermediate than in the beginning and end periods (Fig 5 (c)).

Precipitation conditions are assessed from laser disdrometer measurements of precipitation and hydrometeor's characteristics at the ENA site (Fig. 6), including precipitation intensity (mm/hour), the number of particles that fall to the surface (counts), the hydrometeors median volume diameter (mm) and the type of precipitation as given by the weather code $w_a w_a$, Table 4680 (WMO, 2015). The beginning of the record displays two heavy precipitation events on May 8th - 9th (days 128 and 129) characterized by very high intensity rain (> 50 mm/hour) and large diameter raindrops (in general > 2 mm). This stormy period is followed by a mostly dry period, with mainly drizzle or low intensity rain and small diameter hydrometeors. The last part of the monitoring period is characterized by drizzle and rain events of moderate intensity, with the exception of an isolated high-intensity precipitation event (> 30 mm/hour) at the end of June 3rd (day 154).

The comparison of the temporal variability of gamma radiation counts (Fig. 3) and of meteorological parameters (Fig. 4 and Fig. 6) confirms the expected influence of atmospheric conditions on the radon progeny concentration in the atmosphere. For example, the most intense precipitation events coincide with sharp peaks in gamma radiation counts, which are absent on the mainly dry period in the middle of the record. However, some precipitation events don't seem to affect the gamma radiation counts (e.g. day 154), and the largest gamma peak (on day 161) is associated with a comparatively low intensity rain event, confirming that further aspects need to be taken into account for a more complete explanation of changes in gamma radiation. Since radon progeny, being mostly positively charged isotopes of heavy metals (bismuth, lead,…) attaches readily to airborne participate matter, aerosols are a further key aspect that needs to be taken into consideration. Figure 7 shows the total aerosol concentration derived from HTDMA measurements at the ENA facility. The time series is dominated by a few events of very large aerosol concentration (> 10 x10^3 particles/cm^3), the largest one occurring on 13th May (day 133) (Fig. 7 (a)).

Apart from these events which are typically very short (a few hours at most), the total aerosol concentration is usually small (Fig. 7(b)), as expected from the marine geographical location and low pollution levels of the monitoring site. The most striking feature is the marked increase in total aerosol concentration at the end of the record, particularly on June 10th (day 161), coinciding with the occurrence of the largest peak in gamma radiation.

The Hybrid Single-Particle Lagrangian Integrated Trajectory (HYSPLIT) 4 model (Stein et al. 2015) is run with NCEP Global Data Assimilation System (GDAS) meteorological data in order to derive daily 3-day back trajectories ending at Graciosa 500m above the ground level. The first part of the record (from days 128 to 134) corresponds to air masses with trajectories coming from North America, the middle part (from days 135 to 160) is associated with more local air masses and recirculating Azores high flow, and days 161-163 are associated with air masses from western Europe, as illustrated in Fig. 8.

3.2. Variability patterns

The short-term variability of gamma radiation is summarized in Table 1 in terms of the percentage magnitude of the corresponding anomalies. The largest anomalies are sharp peaks lasting typically 2-4 hours, while the broader peaks correspond to smaller variations in gamma counts and have a diurnal pattern with an increase in the first hours of the day, reaching a maximum in the early morning and decreasing again to a minimum in the evening. The sharp peaks are associated with strong precipitation events (except for day 133), while the diurnal peaks are related mainly with dry periods (except for day 154).

The concurrence of sharp anomalies in gamma radiation and heavy rain is confirmed by the detail plot in Figure 9. For the three largest peaks (days 128, 129 and 161) the sharp increase in gamma radiation is coincident with a rain event, with high counts persisting for about 30-45 minutes after the rain ends. Furthermore, the peaks are asymmetric, decreasing slower and returning to a slightly lower level than before the anomaly. The magnitude of the largest peak on day 161 corresponds to a comparatively lower precipitation intensity, but a significantly larger concentration of aerosols below 700 nm (Fig. 10). Day 161 is also characterized by the largest heights of the nocturnal PBL (Fig. 5). In contrast the peak on day 133 is wider and exhibits an opposite behavior, increasing slower than the corresponding decrease. Furthermore, while the start of the anomaly seems to coincide with heavy rain in the early morning, the maximum is only reached about 3 hours later (around 08:30), coincident with very high concentration of aerosols (Fig. 10).

Two events of heavy precipitation, at the end of day 154 (3rd June), starting around 22:30 and exceeding 30 mm/hour, and at the end of day 159 (8th June), starting around 18:30 and exceeding 15 mm/hour, are not associated with concurrent peaks in gamma radiation counts. A possible explanation is the type of precipitation being of convective type for these events. This is supported by the time series of convective available potential energy, an indicator of convective activity, displayed in Fig. 11. The two largest values of CAPE, associated with strong atmospheric instability, occur for these same two days (3rd and 8th June). These two precipitation events are

also characterized by a large number of large volume particles (Fig. 6).

The small diurnal cycles are observed in dry conditions and weak winds (Fig. 4(c)), indicating that they are associated with the stability of the atmosphere and the diurnal cycle of the planetary boundary layer. This is illustrated by the detailed time series shown in Figure 12. For day 141 the peak in gamma counts is coincident with very low wind speed around 06:30 and starts to decrease before 07:00 when the air temperature starts to increase. Weak winds are also observed during the night of day 156, but the temperature starts to increase earlier, around 04:00, and gamma counts start to decrease also earlier (Fig. 12). The radon gas is able to accumulate near the surface in situations of calm winds during the night and weak turbulence conditions, but mixing due to thermal turbulence starts to decrease the concentration of radon gas near the ground when temperature starts to increase. This explanation for the diurnal variability is in agreement with previous work reporting the build-up of radon during the night as associated with the formation of a stable nocturnal boundary layer and depletion during the day as the result of near surface convection and the formation of a convective boundary layer (Pascale et al, 2014). Day 154 seems an exception in the sense that the diurnal cycle is observed on a non-dry day. However, the early hours of the day are characterized by weak winds, and the same situation of radon gas accumulation before sunrise takes place. Intense precipitation (> 30 mm/h) only starts after 22h00, and thus not affects the diurnal variability of gamma radiation.

Troughs occur less frequently and have much smaller magnitude than positive anomalies. The larger troughs (on days 155 and 160 - 4th and 9th June) occur after heavy precipitation of convective type. Negative departures from the average also occur after heavy non-convective precipitation, but are of even smaller magnitude and have shorter duration.

4. Discussion and conclusions

The interpretation of the temporal variability of gamma radiation requires a detailed examination of the origin of the gamma rays that are being measured. Given the experimental set-up of the monitoring campaign, with the sensor placed 1m above the ground without any lead shielding below, the sensor is able to measure both gamma rays from the atmosphere and from the surface including gamma rays from the first ~30 cm of the soil layer. Although a sharp distinction between terrestrial and atmospheric sources of gamma rays is not possible with the current set-up, the surface contribution is expected to be the dominant, given the much larger concentration of gamma emitting radionuclides in the surface than in the atmosphere. Furthermore, being largely comprised by gamma rays originating inside mineral grains, the terrestrial gamma radiation is expected to be stabler in time. Two main physical processes contribute to temporal changes in the surface contribution: radon gas transport inside the porous medium (dependent on soil and meteorological parameters) and attenuation of gamma rays associated with soil moisture (Yoshioka, 1994). The atmospheric contribution from radon progeny in the near surface or brought down from the upper atmosphere by precipitation scavenging is expected to produce sharper and faster variability in gamma radiation.

The temporal variability of gamma radiation measured at the ENA facility is characterized by occasional peaks over a slowly-varying signal. The long-term signal is interpreted as originating from gamma radiation from the surface, while the peaks are considered to be driven mainly by atmospheric sources. The sharp peaks that dominate the short-term variability of gamma radiation during the monitoring period are coincident with heavy precipitation events, therefore resulting from the scavenging effect of precipitation bringing radon progeny from the upper air to the ground surface. The persistence of high gamma counts for about 30-45 minutes after the rain stops is consistent with the half-lives of gamma-emitting radon progeny Pb-214 (27 min), and Bi-214 (20 min). The return of gamma counts to a slightly lower level after the heavy rain can be explained by the high water content of the ground. The increase in soil moisture associated with rain (and consequent reduction in soil permeability) causes first a decrease in the exhalation of radon gas from the soil to the atmosphere and then due to water infiltration a decrease in radon concentration associated with dilution of Rn gas and migration to deeper levels (Pascale et al, 2015). Furthermore, the gamma rays from all gamma-emitting elements in the ground are attenuated by the presence of water in the medium (Yoshioka, 1994). Both effects contribute to a decrease in gamma radiation following precipitation events. These same processes can explain the troughs in gamma counts as observed in days 155 and 160, since these occur after heavy precipitation with consequent increase of the water content of the surface.

Despite the obvious role played by precipitation on the short-term variability of gamma radiation, the connection is far from being straightforward as a result of the complex interplay of factors such as the precipitation intensity, the PBL height, the cloud's base height and thickness, or the air mass origin and atmospheric concentration of aerosols, which influence the scavenging processes affecting the concentration of radon progeny. The dominant mechanism of scavenging of radon progeny from the atmosphere by precipitation is expected to be within the cloud rather than below-cloud wash-out (Fujinami, 1996), since the radon progeny attaches mostly to aerosols with a diameter of a few hundred nanometres which are prone to nucleation scavenging and other in-cloud processes but are not subject to impaction by falling hydrometeors (Paatero and Hatakka, 1999). Wash-out is strongly dependent on the cloud base height since the drops falling through a larger distance are able to catch more progeny by below-cloud wash-out.

As an illustration, the precipitation events on days 128 and 129 have similar characteristics in terms of air mass history, precipitation intensity, and number and volume of particles, but originate peaks in gamma radiation roughly half the magnitude, as a result of the larger thickness and cloud base height of clouds in day 128 compared to day 129, and consequent higher efficiency of below-cloud wash-out. However, in both cases the slower decreasing of gamma rays is in agreement with model results for the radiation resulting from in-cloud scavenging (Horng and Jiang, 2003), indicating a dominant contribution from rainout processes to the observed enhancement in gamma radiation. The largest peak in gamma radiation on day 161 occurs for a much less intense precipitation event, but a very large concentration of fine aerosols associated with the arrival of an air mass from western Europe. Day 161 is also characterized by very high nocturnal PBL enabling

radon gas at the near surface to be mixed up to higher levels. The sharp peak on day 133 coincides with a even less intense precipitation event but also high concentration of aerosols. The distinct shape of the anomaly (slower increase) and the high cloud base suggests that below-cloud wash-out is the dominant process in this case.

Enhancements in gamma radiation occurring in the absence of precipitation and already reported in previous studies (Inomata et al. 2017; Yakovleva et al. 2016) are here attributed to nocturnal atmospheric conditions of low winds and air temperature enabling the build-up of near surface radon progeny during the night. These diurnal signals have a typical shape (maximum at dawn or early morning and typically duration exceeding 6 hours) but magnitudes comparable to rain-induced peaks, so the distinction between the two types of gamma radiation enhancement enhancement can be challenging, particularly in the case of data with low temporal resolution.

As also previously reported (Yakovleva et al. 2016) some precipitation events don't produce detectable effects in gamma radiation. Although this was interpreted as an artifact resulting from the local nature of precipitation and the distance between the meteorological station and the gamma monitoring site, here this effect is undoubtedly observed with co-located gamma and meteorological measurements, in conditions of convective precipitation (for example at the end of day 154). In the case of convective precipitation associated with cumuliform clouds forming under conditions of warmer ground than the air, the dominant microphysical mechanism is the faster accretion of liquid water. Thus in the drop growing process leading to convective rain, the addition of water results in a reduction of the concentration of radionuclides by dilution, explaining the lack of sharp peaks in gamma radiation. In contrast dynamically active cumuliform clouds forming behind a cold front rather than by warm updraft resulting from warming of the ground relative to the air (as is the case in day 128) produce enhancements in gamma radiation due to the ability of slowly growing cloud condensation nucleus and consequent nucleation scavenging of radon progeny.

In addition to radon gas exhalation from the ground, the source of radon progeny in the air has a remote component resulting from aerosols and condensation nuclei in upper levels, and can have an additional local component resulting from wind transport and/or updraft of radon gas from the Graciosa surface. As a result of the geographical location of the site, in the middle of the Atlantic ocean, and given the natural land/ocean contrast in radon gas concentration, the local contribution is expected to be smaller than the remote component. Advance on the understanding of the relative importance of these components, as well as on the distinction between below-cloud washout and in-cloud processes, could be obtained by means of simultaneous measurements of radon progeny concentration in air and in the precipitation itself, which unfortunately are not available. Continuous monitoring of atmospheric radon would be also extremely valuable, since significant disequilibrium between Rn-222 and its progeny is expected to occur on all time scales, including sub-synoptic time scales (Zahorowski et al. 2012). Further insight is expected to be gained by extending the monitoring set-up to include additional alpha particle sensors, given the advantages of the combination of the two types of measurements (Zafrir et al. 2011, 2013) for the

understanding of the temporal variability of radon and its progeny.

Acknowledgments

The invaluable technical assistance of Mr Carlos Sousa, Mr Bruno Cunha and Mr Tércio Silva from the ARM-ENA facility is gratefully acknowledged. Data were obtained from the Atmospheric Radiation Measurement (ARM) Program sponsored by the U.S. Department of Energy, Office of Science, Office of Biological and Environmental Research, Climate and Environmental Sciences Division. The authors gratefully acknowledge the NOAA Air Resources Laboratory (ARL) for the provision of the HYSPLIT transport and dispersion model. H. Woith, H. Zafrir and H. Silva are thanked for valuable discussions on the manuscript. This work is financed by the ERDF – European Regional Development Fund through the Operational Programme for Competitiveness and Internationalisation - COMPETE 2020 Programme, and by National Funds through the FCT – Fundação para a Ciência e a Tecnologia (Portuguese Foundation for Science and Technology) within project POCI-01-0145-FEDER-006961.

References

Arnold, D., Vargas, A., Vermeulen, A. T., Verheggen, B., Seibert, P. 2009. Analysis of radon origin by backward atmospheric transport modelling. Atmos. Environ. 44, 494-502.

Barbosa, S.M., Donner, R.V., Steinitz, G. 2015. Radon applications in geosciences - progress & perspectives. Eur. Phy. J. Special Topics 224, 597-603.

Brunetti, M., Cecchini, S., Galli, M., Giovannini, G., Pagliarin, A. 2000. Gamma-ray bursts of atmospheric origin in the MeV energy range. Geophys. Res. Lett. 27, 1599-1602.

Burnett, J.L., Croudace, I.W., Warwick, P.E. 2010. Short-lived variations in the background gamma-radiation dose. J. Radiological Prot. 30, 525.

Chambers, S., Zahorowski, W., Matsumoto, K. and Uematsu, M., 2009. Seasonal variability of radon-derived fetch regions for Sado Island, Japan, based on 3 years of observations: 2002–2004. Atmos. Environ. 43, 271-279.

Chambers, S.D., Zahorowski, W., Williams, A.G., Crawford, J., Griffiths, A.D. 2013. Identifying tropospheric baseline air masses at Mauna Loa observatory between 2004 and 2010 using radon-222 and back trajectories. J. Geophy. Res. Atmos. 118, 992-1004.

Cleveland, W.S. 1979. Robust Locally Weighted Regression and Smoothing Scatterplots. J. Am. Stat. Assoc. 74, 829-836.

Dorman, L., 2013. Cosmic Rays in the Earth's atmosphere and underground. Springer, New York.

Dong, X., Xi, B., Kennedy, A., Minnis, P., Wood, R., 2014. A 19-month record of marine aerosol cloud radiation properties derived from DOE ARM mobile facility deployment at the Azores. Part I:

cloud fraction and single-layered MBL cloud properties. J. Clim. 27, 3665-3682.

Fujinami, N. 1996. Observational study of the scavenging of radon daughters by precipitation from the atmosphere. Environ. Int. *22*, 181-185.

Härdle, W., Steiger, W. 1995. Optimal median smoothing. Applied Statistics 44, 258-264.

Horng, M.C. and Jiang, S.H. 2003. A rainout model for the study of the additional exposure rate due to rainfall. Radiati. Meas. *37,* 603-608.

Inomata, Y., Chiba, M., Igarashi, Y., Aoyama, M., Hirose, K. 2007. Seasonal and spatial variations of enhanced gamma ray dose rates derived from 222Rn progeny during precipitation in Japan. Atmos. Environ. 41, 8043 – 8057.

Levin, Z. and Cotton, W.R. eds., 2008. Aerosol pollution impact on precipitation: a scientific review. Springer, New York.

Logan, T., Xi, B., Dong, X. 2014. Aerosol properties and their influences on marine boundary layer cloud condensation nuclei at the ARM mobile facility over the Azores. J. Geophy. Res. Atmos. 119, 4859-4872.

Mann, J. A., Chiu, J.C., Hogan, R.J., O'Connor, E.J., L'Ecuyer, T S., Stein, T. H., Jefferson, A., 2014. Aerosol impacts on drizzle properties in warm clouds from ARM Mobile Facility maritime and continental deployments. J. Geophys. Res. Atmos. 119*,* 4136-4148.

Mercier, J.-F., Tracy, B.L., d'Amours, R., Chagnon, F., Hoffman, I., Korpach, E.P., Johnson, S., Ungar, R.K., 2009. Increased environmental gamma-ray dose rate during precipitation: a strong correlation with contributing air mass. J. Environ. Radioactiv. 100, 527 – 533.

Minato, S., 1980. Analysis of time variations in natural background gamma radiation flux density. J. Nucl. Sci. Technol. 17, 461-469.

Nishikawa, T., Okabe, S., Aoki, M. 1989. Monte carlo calculation of gamma-ray flux density due to atmospheric radon daughters. J. Nucl. Sci. Technol. 26, 525-529.

Nitschke, K., Azevedo, E., Ortega, P., Haruta, A. 2014. Eastern North Atlantic (ENA) Graciosa Island - ARM Facility. Geophys. Res. Abstr. 16, 6077.

Paatero, J., Hatakka, J. 1999. Wet deposition efficiency of short-lived radon-222 progeny in central Finland. Boreal Env. Res. 4, 285-293

Pascale, F. T., De Francesco, S., De Carbone, P., Cuoco, E. and Tedesco, D. 2014. Dry soil diurnal quasi-periodic oscillations in soil 222Rn concentrations. Radiat. Meas. 66, 31-41.

Pascale, F.T., Carbone, P., De Francesco, S., Cuoco, E. and Tedesco, D. 2015. Rainstorm-induced soil 222Rn concentration spikes observed in Southern Italy. Environ. Earth Sci. 73, 8177-8187.

Rémillard, J., Kollias, P., Luke, E., Wood, R. 2012. Marine boundary layer cloud observations in the Azores. J. Climate, 25, 7381-7398.

Sesana, L., Ottobrini, B., Polla, G., Facchini, U. 2006. 222-Rn as indicator of atmospheric turbulence: measurements at Lake Maggiore and on the pre-Alps. J. Environ. Radioactiv. 86, 71 – 288.

Stein, A.F., Draxler, R.R, Rolph, G.D., Stunder, B.J.B., Cohen, M.D., Ngan, F. 2015. NOAA's HYSPLIT atmospheric transport and dispersion modeling system. Bull. Amer. Meteor. Soc. 96, 2059-2077.

Takeuchi, N., Katase, A. 1982. Rainout-washout model for variation of environmental gamma-ray intensity by precipitation. J. Nucl. Sci. Technol. 19, 393-409.

Zafrir , H., Haquin, G., Malik, U., Barbosa, S.M., Piatibratova, O., Steinitz, G., 2011. Gamma versus alpha sensors for Rn-222 long-term monitoring in geological environments. Radiat. Meas. 46, 611-620.

Zafrir, H., Barbosa, S. M., Malik, U., 2013. Differentiation between the effect of temperature and pressure on radon within the subsurface geological media. Radiat. Meas. 49, 39-56.

Whittlestone, S., Robinson, E., & Ryan, S. 1992. Radon at the Mauna Loa Observatory: Transport from distant continents. Atmos. Environ. 26, 251-260.

Wilkening, M. 1981. Radon in atmospheric studies: a review. In Second Special Symposium, Bhabha Atomic Research Center Bombay, CONF-810153-3 DE93, vol. 3345.

Williams, A.G., Chambers, S., Griffiths, A. 2013. Bulk mixing and decoupling of the nocturnal stable boundary layer characterized using a ubiquitous natural tracer. Bound-Lay Meteorol. 149, 381-402

WMO, 2015.Manual on Codes, WMO-No. 306, WMO, Geneva, Switzerland

Wood, R., Bretherton, C., Albrecht, B., Coe, H., Fairall, C., Garreaud, R., Ackerman, T., Stevens, B., Feingold, G., Turner, D. 2009. Clouds, Aerosol, and Precipitation in the Marine Boundary Layer (CAP-MBL) Science Plan for the 2009/2010 Deployment of the ARM Mobile Facility to Graciosa Island, the Azores, NE Atlantic, DOE/SC-ARM-0902.

Wood, R. 2012. Stratocumulus clouds. Mon. Weather Rev. 140, 2373-2423.

Wood, R., Wyant, M., Bretherton, C.S., et al. 2015. Clouds, Aerosols, and Precipitation in the Marine Boundary Layer: An ARM Mobile Facility Deployment. Bull. Amer. Meteor. Soc. 96, 419-440.

Yakovleva, V.S., Nagorsky, P.M.,Cherepnev, M.S., Kondratyeva, A.G., Ryabkina, K.S. 2016. Effect of precipitation on the background levels of the atmospheric beta- and gamma-radiation. Applied Radiat. Isotopes 118, 190-195

Yoshioka, K. 1994. Study of time variation of terrestrial gamma radiation due to depth distribution of soil moisture content. Radioisotopes 43, 183-189.

Zahorowski, W., Chambers, S., Crawford, J., Williams, A.G., Cohen, D.D., Vermeulen, A.T., Verheggen, B. 2012. 222Rn observations for climate and air quality studies. In Sources and measurements of radon and radon progeny applied to climate and air quality studies, Proceedings

Series - International Atomic Energy Agency, STI/PUB/1541.

Day	Date	%variation counts	~time of max	~duration	Rain (mm/hour)	Aerosol ($1/cm^3$)
161	10/06/2015	7%	12:00	4h	>10	217
128	08/05/2015	6%	07:00	2h	>50	46
129	09/05/2015	3%	13:00	4h	>50	38
133	13/05/2015	3%	08:30	5h	<10	883
142	22/05/2015	3%	06:00	>6h	0	66
141	21/05/2015	2.5%	06:00	>6h	0	95
154	03/06/2015	2.5%	02:30	>6h	>30	98
153	02/06/2015	2%	06:30	>6h	0	140
150	30/05/2015	1.5%	06:30	>6h	<3	71
156	05/06/2015	1.5%	04:00	>6h	0	115

Table 1: Characteristics of gamma anomalies, precipitation intensity, and daily averaged aerosol concentration.

List of Figures

Figure 1: Geographical location of the ARM-ENA facility at the Graciosa island, Azores archipelago.

Figure 2: Time series of gamma counts (points) and long-term signal (solid line).

Figure 3: Detrended time series of gamma counts variation.

Figure 4: Time series of 1-min surface meteorological observations at the ENA facility.

Figure 5: Summary plots of median (horizontal thick line), 1st quartile (Q1, lower edge of box) and 3rd quartile (Q3, upper edge of box) values: (a) cloud base height, (b) cloud thickness (cloud top - cloud base), and (c) planetary boundary layer height (PBLH).

Figure 6: Time series of precipitation characteristics from laser disdrometer measurements: (a) precipitation intensity (mm/hour), (b) number of aqueous particles detected at the surface (counts), (c) median volume diameter of particles (mm) and (d) precipitation type from $w_a w_a$ weather code.

Figure 7: Time series of total aerosol concentration from HTDMA measurements: (a) full range and (b) zoom.

Figure 8: Trajectory maps (upper panels) and heights (lower panels) for 3-day airmass back-trajectories ending at Graciosa 500m above ground level: day 133 (top), day 141 (middle), and day 161 (bottom).

Figure 9: Detail time series of gamma anomalies (+) and precipitation intensity (mm/year).

Figure 10: Concentration of aerosol from the HTDMA instrument.

Figure 11: Time series of CAPE (convective available potential energy) from microwave radiometer profiler.

Figure 12: Detail time series of gamma anomalies (+) and atmospheric parameters (air temperature, and wind speed) for two individual days: (a) day 141 (21/05/2015); (b) day 156 (05/06/2015).

Figure 1: Geographical location of the ARM-ENA facility at the Graciosa island, Azores archipelago.

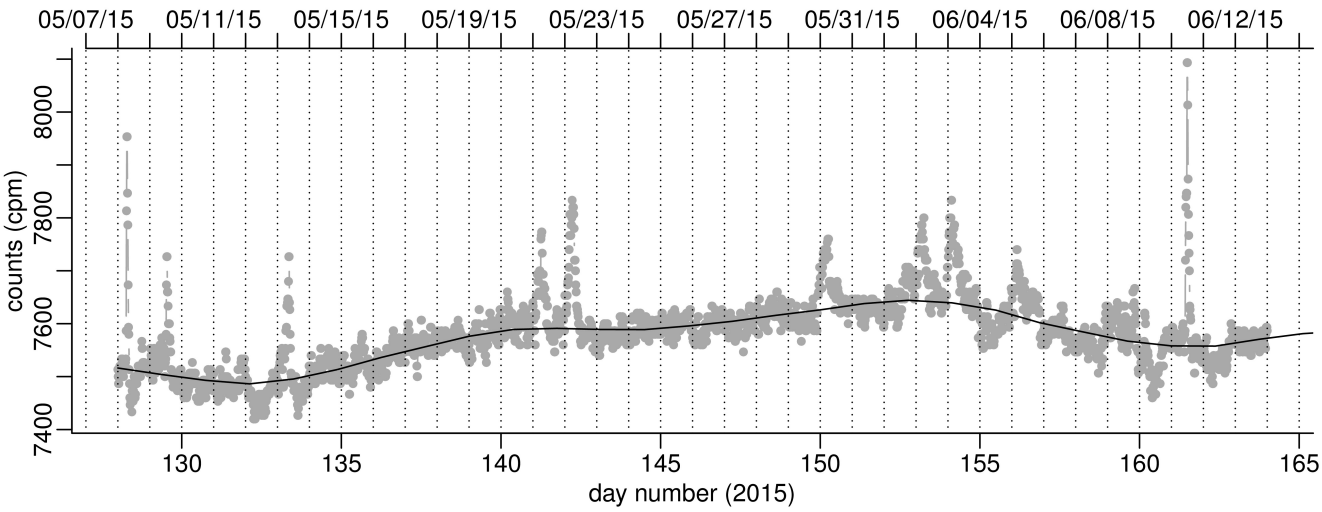

Figure 2: Time series of gamma counts (grey) and long-term signal (black line).

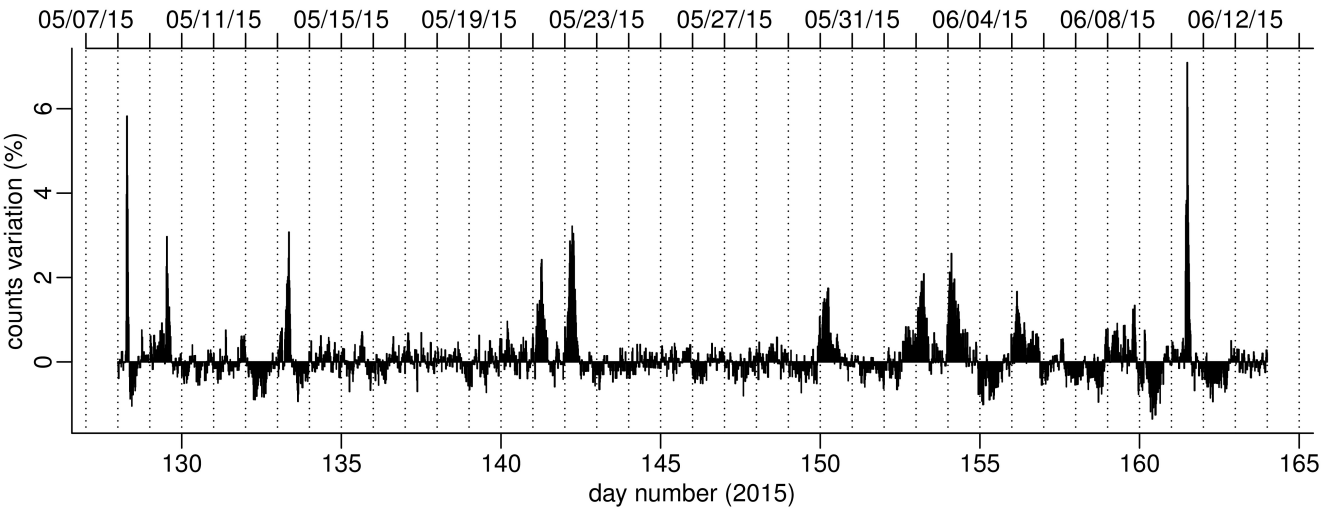

Figure 3: Detrended time series of gamma counts variation.

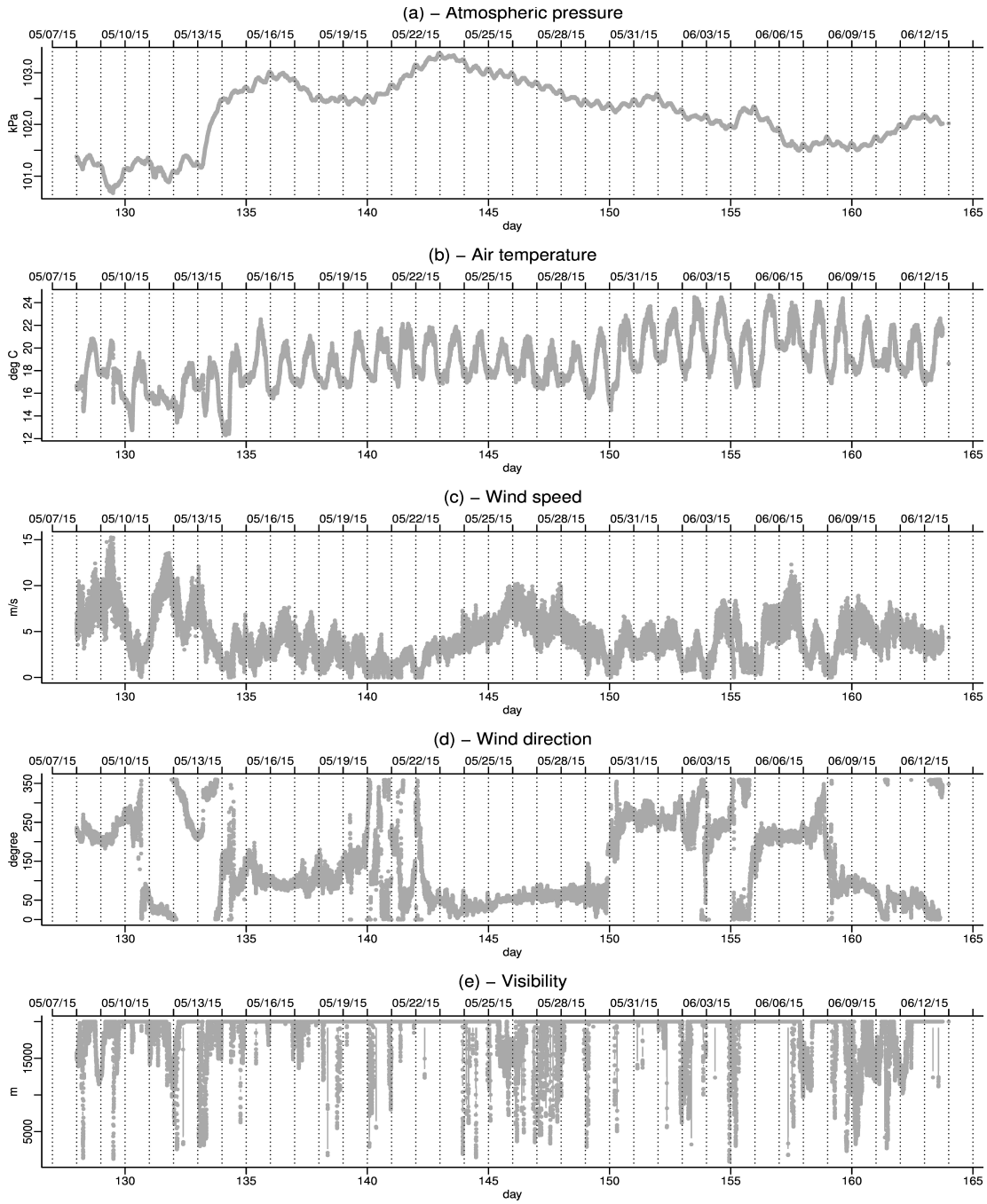

Figure 4: Time series of 1-min surface meteorological observations at the ENA facility.

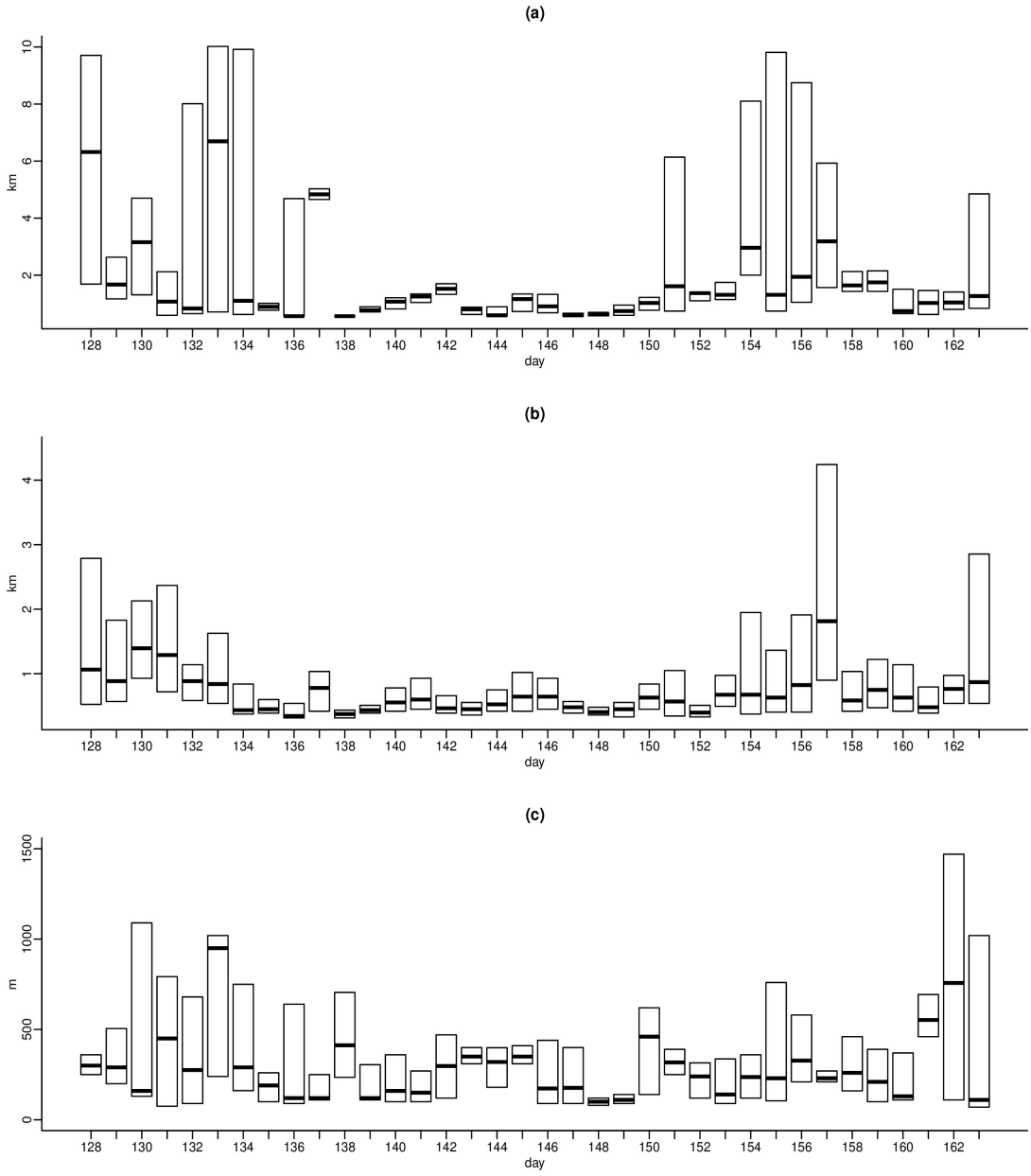

Figure 5: Summary plots of median (horizontal thick line), 1st quartile (Q1, lower edge of box) and 3rd quartile (Q3, upper edge of box) values: (a) cloud base height, (b) cloud thickness (cloud top - cloud base), and (c) planetary boundary layer height (PBLH).

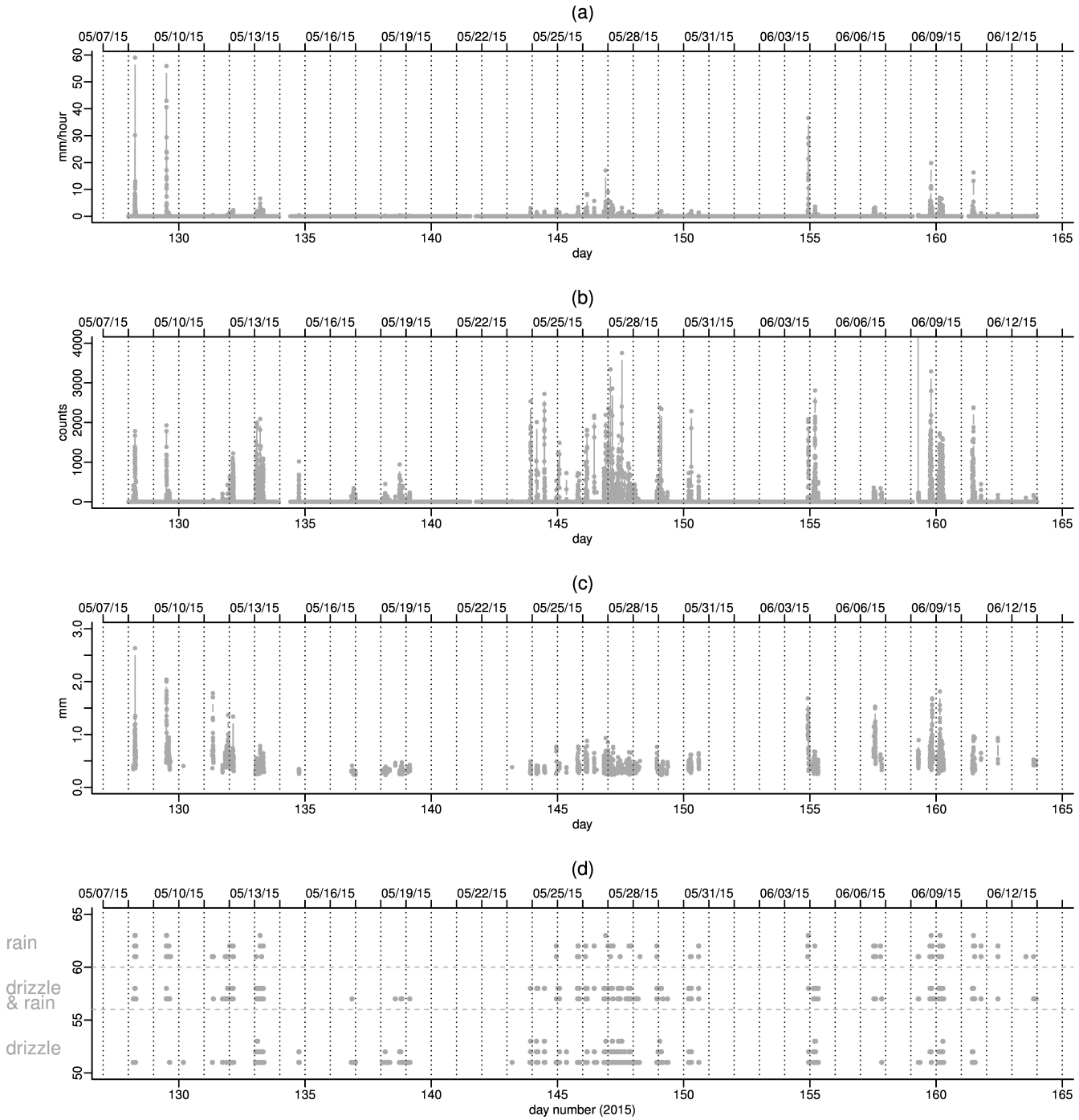

Figure 6: Time series of precipitation characteristics from laser disdrometer measurements: (a) precipitation intensity (mm/hour), (b) number of aqueous particles detected at the surface (counts), (c) median volume diameter of particles (mm) and (d) precipitation type from $w_a w_a$ weather code.

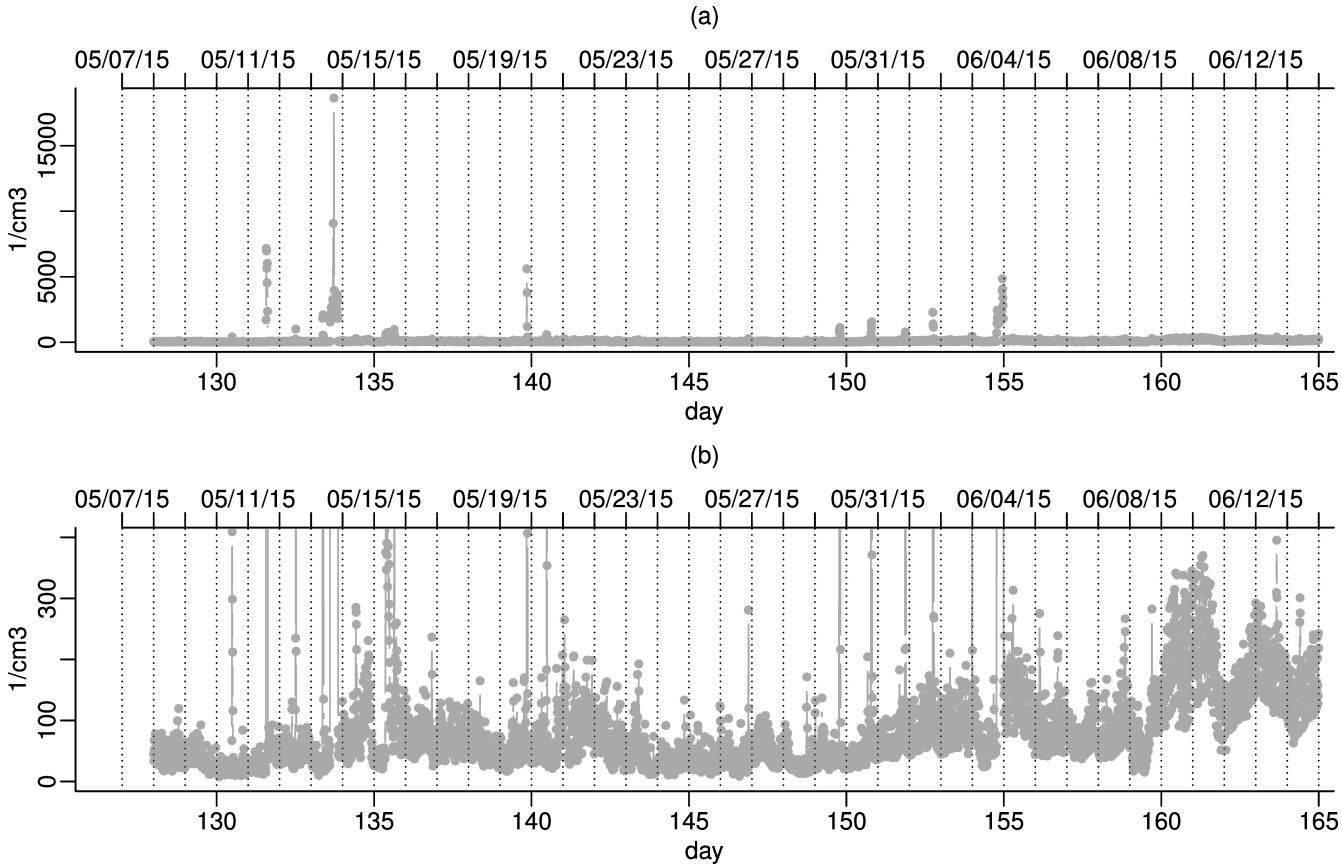

Figure 7: Time series of total aerosol concentration from HTDMA measurements: (a) full range and (b) zoom.

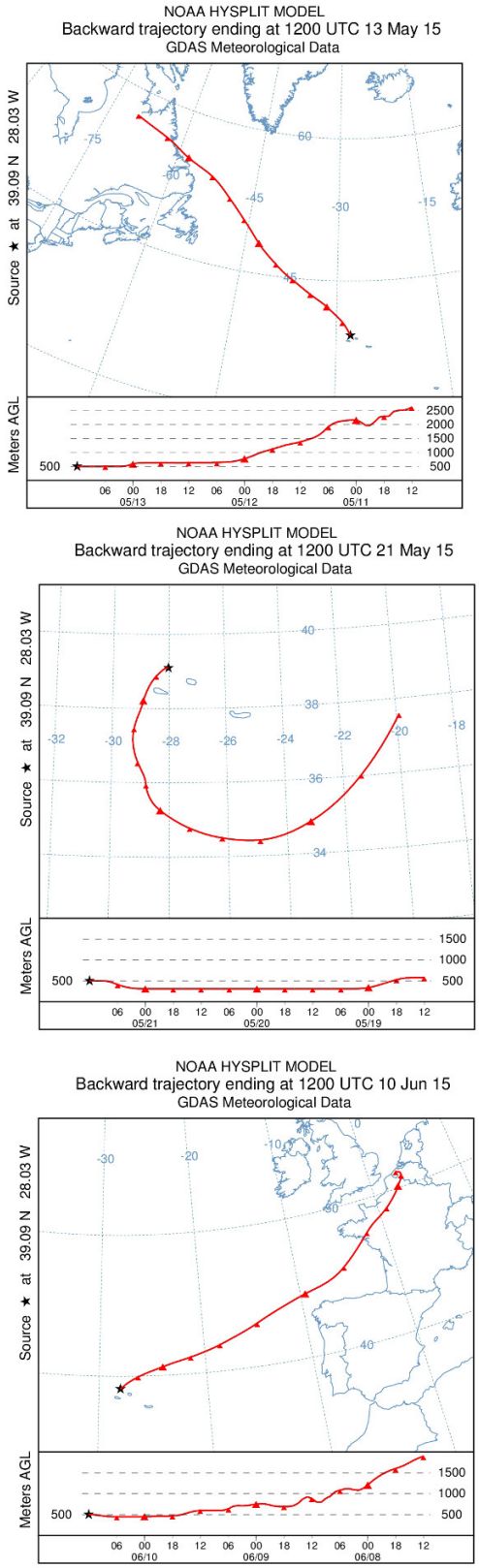

Figure 8: Trajectory maps (upper panels) and heights (lower panels) for 3-day airmass back-trajectories ending at Graciosa 500m above ground level: day 133 (top), day 141 (middle), and day 161 (bottom).

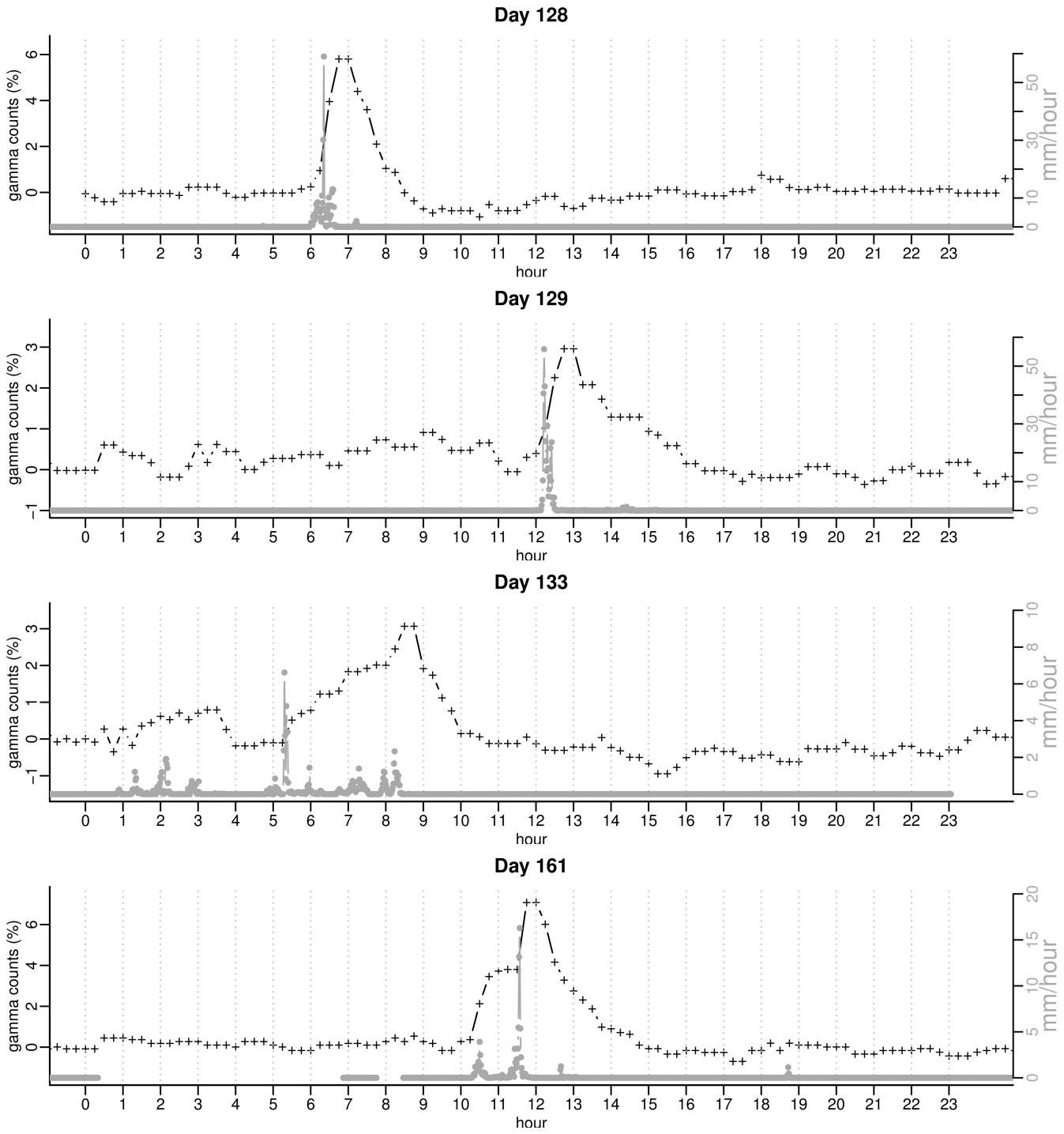

Figure 9: Detail time series of gamma anomalies (+) and precipitation intensity (mm/year).

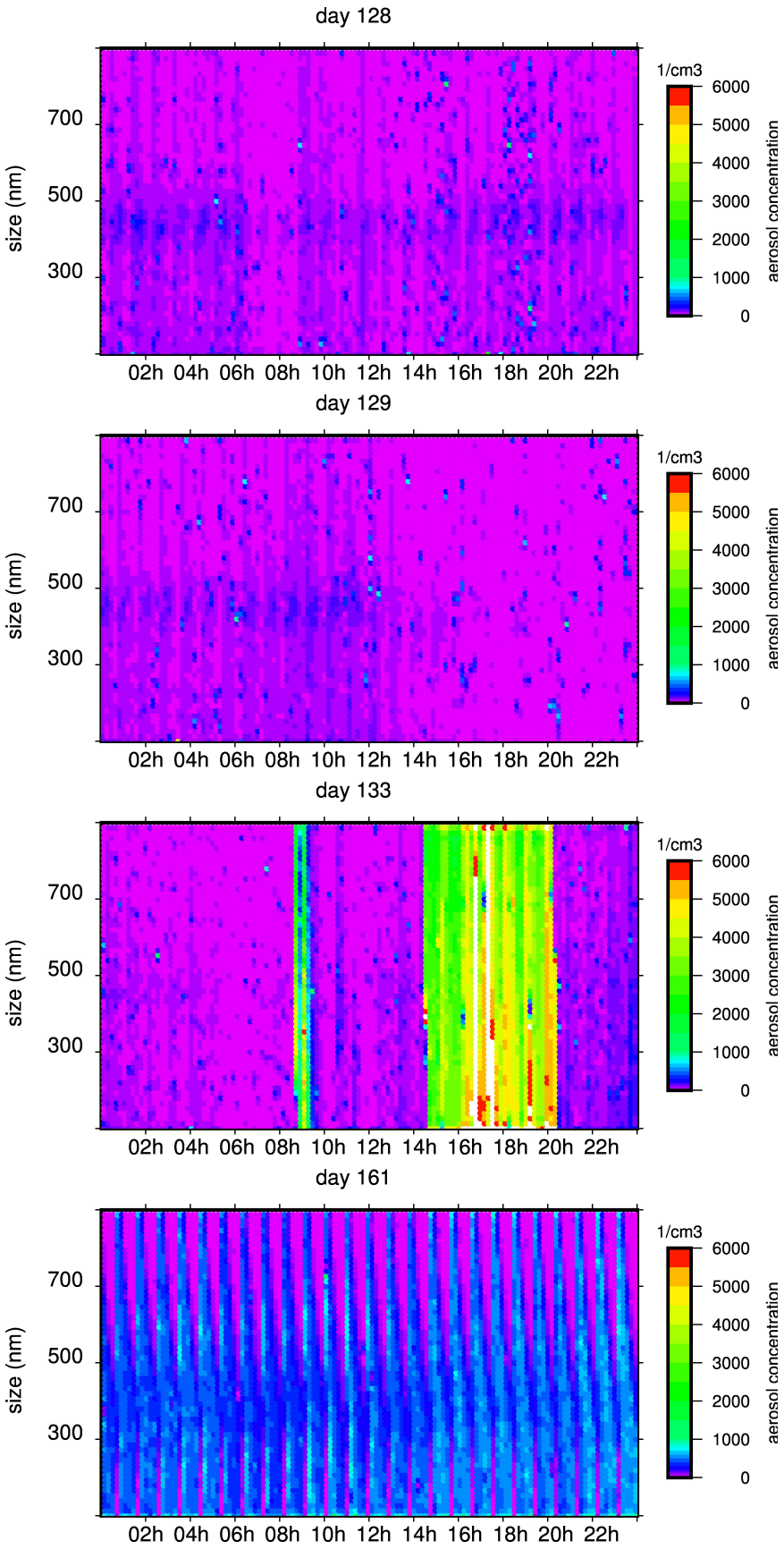

Figure 10: Concentration of aerosol from the HTDMA instrument.

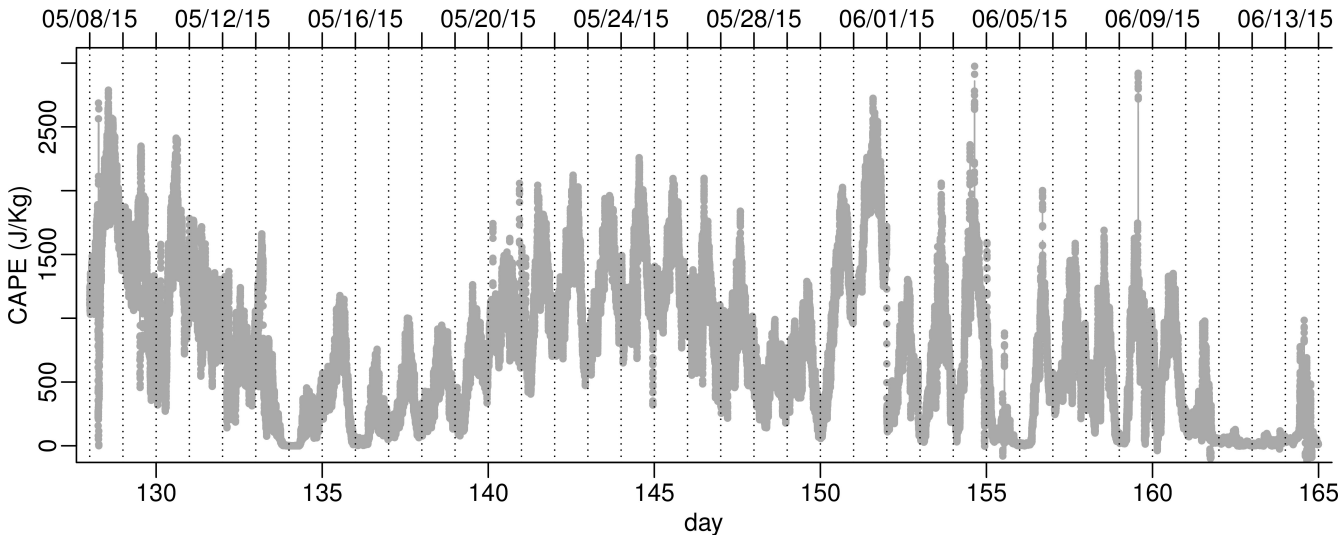

Figure 11: Time series of CAPE (convective available potential energy) from microwave radiometer profiler.

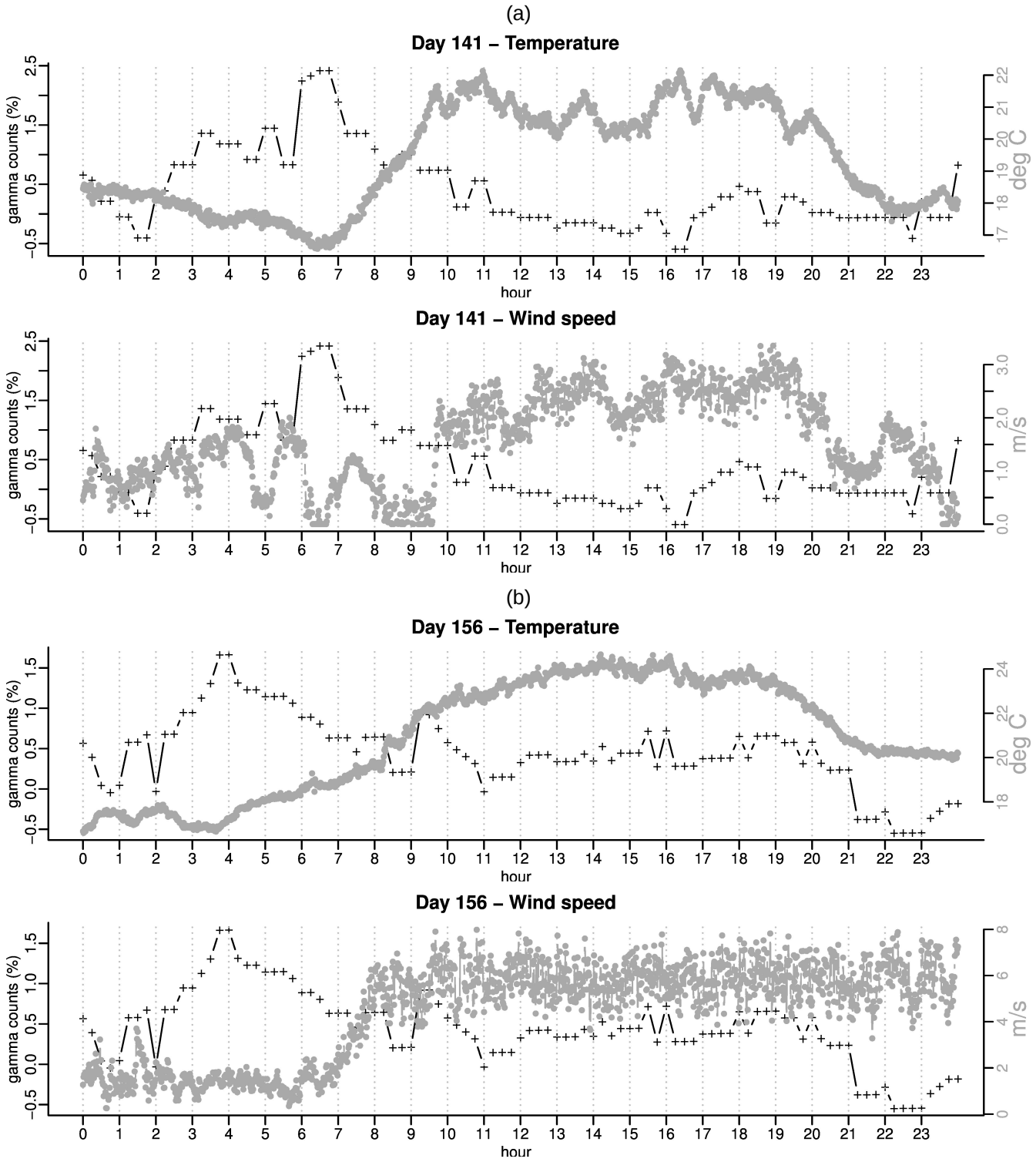

Figure 12: Detail time series of gamma anomalies (+) and atmospheric parameters (air temperature, and wind speed) for two individual days: (a) day 141 (21/05/2015); (b) day 156 (05/06/2015).